Applied Catalysis B: Environmental 324 (2023) 122183

Contents lists available at ScienceDirect

Applied Catalysis B: Environmental

journal homepage: www.elsevier.com/locate/apcatb

Photocatalytic water splitting of improved strontium titanate for simultaneous separation of H_2 in a twin photoreactor

Yu-Yang Tai [a], Jeffrey C.S. Wu [a,*], Wen-Yueh Yu [a], Marjeta Maček Kržmanc [b,*], Eugene Kotomin [c]

[a] Department of Chemical Engineering, National Taiwan University, Taipei 10617 Taiwan
[b] Advanced Materials Department, Jožef Stefan Institute, Jamova 39, SI-1000 Ljubljana, Slovenia
[c] Institute of Solid State Physics, University of Latvia, 8 Kengaraga str., LV-1063 Riga, Latvia

ARTICLE INFO

Keywords:
Perovskite
Water splitting
Isopropanol degradation
Z-scheme
Photo twin reactor

ABSTRACT

A core-shell structural Rh-CrO_x loaded on Al^{3+} doped strontium titanate was used for photocatalytic water splitting. A specially designed twin photoreactor, which integrates the water splitting and the degradation of isopropanol, can simultaneously carry out the degradation of isopropanol and hydrogen production. A flux method was conducted to prepare Rh@CrO_3 cocatalyst on Al^{3+} doped high-crystallinity strontium titanate for the photocatalyst of hydrogen evolution. Nearly 1200 μmole/g of hydrogen was evolved in photocatalytic whole water splitting in five hours under simulated AM 1.5 G sunlight. Pt-loaded WO_3 was utilized to degrade 100 ppm isopropanol solution. The above photocatalysts were used in the twin reactor with electron-mediator I^-/IO_3^- and a Neosepta anion-exchanged membrane. Hydrogen evolution of 1102 μmole/g and isopropanol removal of 10.1% were achieved in five hours, indicating the rate-limiting H_2 rate was overcome. The quantum efficiencies on the hydrogen-evolution and degradation sides were estimated to be 0.102% and 0.123%, respectively.

1. Introduction

Nowadays, due to the burning of fossil fuels, global warming and the rising sea level have threatened the creatures on the earth. Many efforts have been made to develop renewable energies like solar, bioenergy, and wind energy to deal with the dilemma. Among all, photocatalysis has been considered a promising technology for utilizing solar energy. Upon photocatalyst absorbing sunlight irradiation with suitable energy, photoinduced electron and hole pairs are initiated and diffused to the surface for possible reactions[1]. In recent research, photoelectrons can behave as the reducing agent for water split into hydrogen [2,3], oxygen reduced into hydrogen peroxide [4,5], or carbon dioxide reduced into hydrocarbons [6]. For photooxidation, photoinduced holes are utilized for the organic compounds degradation [7], water split into oxygen [8], or water oxidized into hydrogen peroxide [9]. Several strategies have been employed in catalyst design to utilize sunlight irradiations further. For example, band position adjustment by heteroatom doping[10,11], defect engineering [12,13], cocatalyst design [14–18], specific facet design [19,20], surface modification [21] and composite design by heterojunction creation [22,23] are potential methods to improve photocatalyst efficiency.

Besides catalyst design, building an artificial photosynthesis system can be another way to boost photocatalytic reactions[24]. In photosynthesis, chloroplast in green plants split water into oxygen and reduces carbon dioxide for sucrose storage in different chambers with the help of enzymes transporting surplus charges or protons. Depending on the transporting route, photocatalysis with electron mediators communicating two different systems is regarded as the Z-scheme system. Fe^{2+}/Fe^{3+} and I^-/IO^{3-} are widely used as electron mediators in artificial photosynthesis. Yu et al.[25] utilized Fe^{2+}/Fe^{3+} as electron mediators to transport surplus charges on Pt/$SrTiO_3$:Rh and $BiVO_4$ between the hydrogen and oxygen evolution sides of the Nafion cation exchange membrane in twin reactors, leading to the separation of products from photocatalytic water splitting. However, in this study, the rate-limiting step was found to be H_2 catalyst waiting for further overcoming in the twin reactor.

In this study, I^-/IO_3^- was chosen as redox pair to mediate surplus photoinduced charges. Strontium titanate with Rh@CrO_3 cocatalyst and Al^{3+} doped was made to perform hydrogen evolution from water splitting on the reduction side in the twin reactor. Cocatalyst, Rh/CrO_3 of core-shell structure, can inhibit the oxidation of H_2 by O_2 and thus significantly improve hydrogen evolution. Thus such catalyst is promising to increase the rate-limiting step in our previous study. On the other side, in semiconductor industries, isopropanol is a typical

* Corresponding authors.
E-mail addresses: cswu@ntu.edu.tw (J.C.S. Wu), marjeta.macek@ijs.si (M.M. Kržmanc).

https://doi.org/10.1016/j.apcatb.2022.122183
Received 28 August 2022; Received in revised form 10 November 2022; Accepted 13 November 2022
Available online 24 November 2022

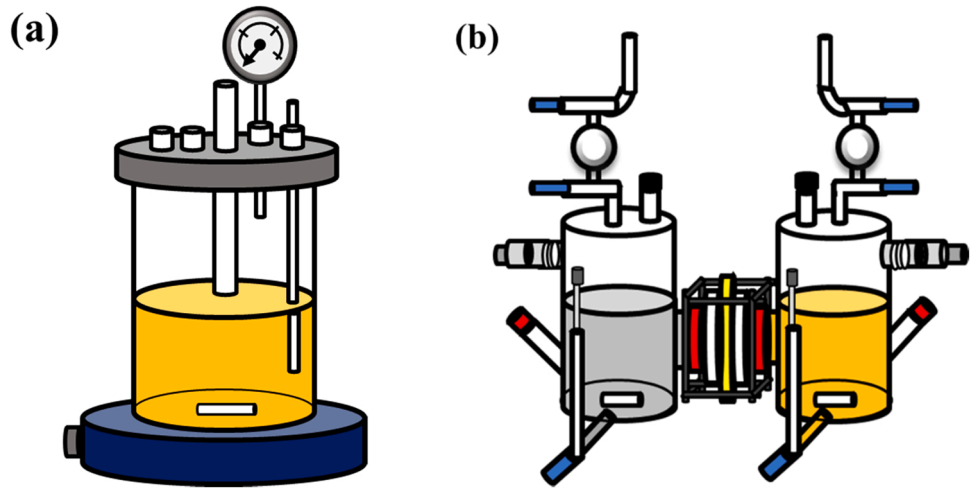

Fig. 1. schematic illustration of (a) single reactor and (b) twin reactors.

wastewater source. To deal with such water pollution, photocatalytic degradation is one of the well-known methods. On the oxidation side, Pt-loaded WO_3 was used for degradation in 100 ppm IPA wastewater. Platinum metal loaded on the tungsten oxide was believed the trap of the photoinduced charges, leading to powerful oxidation in the IPA water solution system. Our objective is to compare the performance of water splitting and IPA photodegradation between the twin and single reactors by catalysts in the condition of half-reaction in a single reactor and overall reaction with mediator pairs in the twin reactors.

2. Experimental

2.1. Synthesis of photocatalysts

For catalysts on the hydrogen evolution side, a molten salt method was performed for $SrTiO_3$ powders with high crystallinity, as reported in the previous literatures[20,26]. 0.01 mol of $SrCO_3$ (Strontium carbonate, Showa Chemical Industry, >99.0%), TiO_2(Titanium oxide, Aldrich, ≧99.5%), $SrCl_2$•6 H_2O (Strontium chloride hexahydrate, VETEC™, ≧99.0%), and Al_2O_3(Aluminum oxide, Alfa Aesar, 99.9%) were uniformly mixed in the elemental molar ratio of 1:1:10:0.01 using a mortar and pestle. The precursors were calcined under 1150 ℃ with a heating rate of 10 ℃/min and annealed for 2 h, then cooled down to room temperature at the rate of 1 ℃/min. After the calcination, the salt was removed from the reacted product by water washing, then drying under 60 ℃ overnight. For the deposition of Rh and Cr, Na_3RhCl_6•12 H_2O (Sodium hexachlororhodate (III) dodecahydrate Rh 17.1%, Alfa Aesar, 99.95%) and $Cr(NO_3)_3$•9 H_2O (Chromium nitrate nonahydrate, Aldrich, 99.0%) were used. The 0.1 wt% of rhodium and chromium elements were loaded by photodeposition and impregnation sequentially[27], respectively, leading to cocatalyst loading in a core-shell structure. First, 300 mg of catalysts were dispersed in 200 mL, 10 vol% methanol solution. A specific amount of Na_3RhCl_6 precursor solution was added by pipette, then irradiated by a 200 W mercury lamp for 2 h. After drying overnight, a mixed solution of dispersed catalyst, 2 mL DI water, and a specific amount of $Cr(NO_3)_3$ precursor solution was prepared for impregnation. A water bath of 80–90 ℃ was used to dry out the solution, and the catalysts were transferred to an alumina crucible. The calcination temperature was set as 350 ℃ with a heating rate of 10 ℃/min and an annealing time of 1 h. The catalysts were denoted as STSC:Al 1150 RC01 after grinding (ST: strontium titanate, SC: strontium chloride, Al: aluminum, 1150:calcination temperature, RC: Rh@CrO_3, 01:0.1 wt% loading). For catalysts on the isopropanol degradation side, the desired amount of platinum precursor (Hexachloroplatinic acid hexahydrate, Sigma Aldrich, 99.95%) was loaded on commercially available WO_3 (Tungsten oxide, Alfa Aesar, 99.8%) by photodeposition method [28].

2.2. Characterization of photocatalysts

The crystal structures of samples were determined by X-ray diffractometer (XRD, Rigaku SmartLab SE) using the X-ray of Cu K_α irradiation (λ = 1.5418 Å). The scanning range fell between 20°~80° with a rate of 10°/min. The UV–vis diffuse reflectance spectra of samples were evaluated by UV/Vis Spectrophotometer (UV-Vis, CARY 300nc, Agilent Technologies) equipped with an integrating sphere. The wavelength range from 200 to 800 nm was measured at a scanning rate of 120 nm/min. And the cutoff wavelength was determined by 350 nm. The morphology of the samples was observed by Field Emission Scanning Electron Microscopy (FE-SEM, Nova™ NanoSEM 230) and High-Resolution Transmission Electron Microscopy (HR-TEM, Cs-corrected STEM, JEOL ARM 200 CF). The surface element analysis was conducted by X-ray Photoelectron Spectroscopy (XPS, Thermo Scientific, Theta Probe).

2.3. Evaluation of photocatalytic activity

The single reactor is illustrated in Fig. 1(a). In this study, first, half-reactions of hydrogen evolution and isopropanol degradation were conducted in a single reactor for parameter optimizations. Based on the abovementioned optimizations, a twin reactor was utilized for Z-scheme reactions, expecting to simultaneously produce hydrogen from water splitting and degrade isopropanol in the wastewater. The light source, a Xenon lamp (Model 66902, Newport) with an AM 1.5 G filter, was calibrated by an optical power meter (Model 843-R, Newport) and thermopile sensor (919 P-003–10, Newport).

For the single reaction of water splitting, 0.1 g of hydrogen evolution catalyst was well dispersed in 200 mL of deionized water. The whole water splitting was performed without sacrificial agent, while a specific amount of NaI was added as the sacrificial agent in the selective water splitting. Sulfuric acid or sodium hydroxide was used for pH value adjustment. Before photocatalysis, the single reactor was purged with argon gas for 20 mins to remove residual air. As for sampling, a gas phase of 0.3 mL was taken every hour and detected by gas chromatography (GC-TCD, China Chromatography; Column: Molecular sieve 5 Å mesh 80/100, Agilent Technologies), using Argon gas as a carrier gas.

For the single reaction of isopropanol degradation, 0.1 g of IPA degradation catalyst was well dispersed in 200 mL, 100 ppm isopropanol water solution. A specific amount of $NaIO_3$ was added as the sacrificial agent. Sulfuric acid or sodium hydroxide was used for pH value adjustment. Before photoreaction, the single reactor was purged

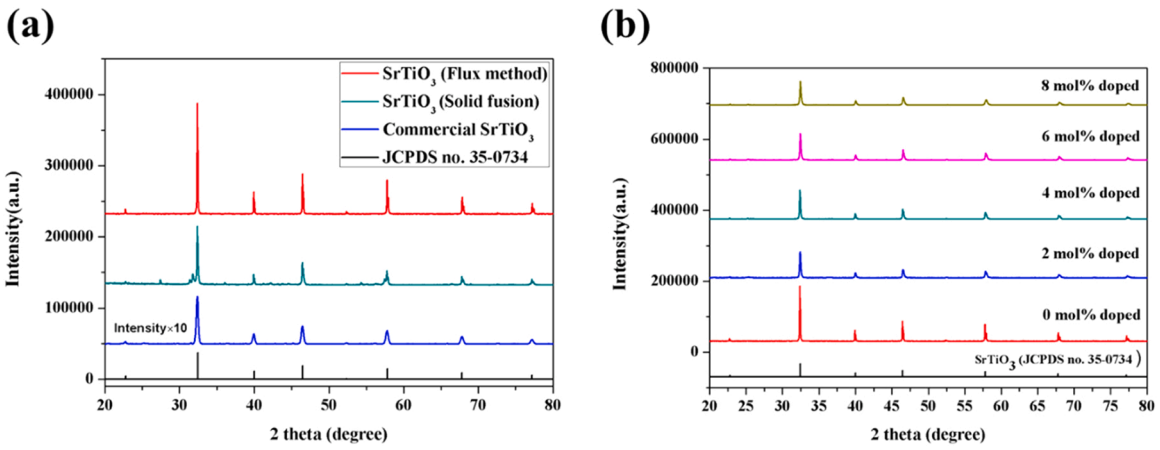

Fig. 2. XRD patterns of (a) $SrTiO_3$ with different synthetic methods and (b) different Al^{3+} doping in flux-mediated $SrTiO_3$.

with argon gas for 20 mins to remove residual air and another 30 mins for absorption-desorption equilibrium. As for sampling, a liquid phase of 1.0 mL was taken every hour and detected by gas chromatography (GC-FID, HP 6890 Series; Column: 19091 N-113, Agilent Technologies) using nitrogen as carrier gas.

The twin reactors are illustrated in Fig. 1(b). The photocatalytic water splitting and isopropanol degradation were coupled in the twin reactors. Two sides were connected and divided by a Neosepta anion exchange membrane (ASTOM). According to the results from single reactors, 0.1 g of hydrogen evolution catalyst, 15 mM of NaI, and 200 mL of deionized water were placed on the hydrogen evolution side, while 0.1 g of IPA degradation catalyst, 15 mM of $NaIO_3$, and 200 mL, 100 ppm IPA water solution were added on the degradation side. Sodium hydroxide was used for pH value adjustment. Before photocatalysis, the twin reactors were purged with argon gas for 20 mins to remove residual air. Liquid-phase composition on the degradation side and gas-phase composition on the hydrogen evolution side were sampled every hour and detected by GC-FID and GC-TCD for five hours.

3. Results and discussion

3.1. Characterization of photocatalyst

Strontium titanate series were used in the hydrogen evolution. Fig. 2 (a) shows the XRD patterns between intrinsic strontium titanate with different synthetic methods, including flux method, solid fusion, and commercial product. The JCPDS no. 35–0734 showed strontium titanate was in a cubic system with perovskite structure. The diffraction peaks fell on $2\theta = 22.8^{\circ}$, 32.4°, 40.0°, 46.5°, 52.4°, 57.8°, 67.8°, 72.5°, 77.2°, especially the (100) facet on $2\theta = 22.8^{\circ}$, which was the dominant exposed facets (shown in Fig.S11) in photocatalytic water splitting for hydrogen evolution [29].

Firstly, the commercially available product showed the lowest crystallinity, which may demonstrate the relation between the low crystallinity of the photocatalyst and low activity. Additional small peaks are found at near $2\theta = 25^{\circ}$ and 30° by solid fusion (green line) in Fig. 2(a). They are unreacted $SrCO_3$ diffraction near at $2\theta = 27^{\circ}$. Furthermore, with the same calcination temperature of 1150 ℃, the strontium titanate with flux method showed outstanding intensity to the solid fusion method. It proves that strontium chloride, as the flux in the system, effectively promoted the dissolution of reactants and reduced diffusion resistance during dissolution and nucleation, leading to ultra-high crystallinity in the lattice. It was expected to lower the charge recombination during charge transportation and increase efficiency. In the absence of flux, inhomogeneous mixture may lead to additional phases like Sr_2TiO_4 and $Sr_4Ti_3O_{10}$ by the solid fusion method. The characteristic peaks of $2\theta = 31.4^{\circ}$ and $2\theta = 32.0^{\circ}$ proved the existence of additional phases in the catalyst by the solid-fusion method. Y. Ham et al. [26] reported that the doping of Al^{3+} could lead to enhancement in photocatalytic activity. Meanwhile, it was well known that doping of heteroatoms caused stress accumulation in lattice and decreased the crystallinity. The doping of Al^{3+} was expected to reduce the average crystal size of strontium titanate due to the smaller size of Al^{3+} compared to Ti^{4+}. Accordingly, in this research, strontium chloride was introduced as the flux to increase solubility between reactants and dopants, hoping to deal with the expected defects after calcination.

Table 1
Comparison of average crystalline size for the catalysts with different Al^{3+} doping amounts.

Catalyst	(110) crystal size (nm)
STSC 1150 0 mol%	73.3
STSC:Al 1150 2 mol%	47.2
STSC:Al 1150 4 mol%	48.8
STSC:Al 1150 6 mol%	54.3
STSC:Al 1150 8 mol%	43.2

The XRD patterns of samples synthesized by different amounts of Al^{3+} are all well-indexed to the cubic structure of strontium titanate (JCPDS no. 35–0734), as shown in Fig. 2(b). Samples doped with Al^{3+} showed relatively lower diffraction intensity than intrinsic strontium titanate. To make a further understanding of the influence of doping amount, Scherrer's equation was considered. The results are summarized in Table 1. It revealed the reduction of average (100) crystal size by Al^{3+} doping, significantly decreasing crystal size from 73 nm to about 40–50 nm, which was supposed to show suppression in the diffusion path of photoinduced charge carriers during photocatalytic reactions. However, there was no apparent tendency with the doping amount toward crystal size.

Fig. 3(a) shows UV–vis spectroscopy ranging from 200 to 800 nm of strontium titanate series with different synthetic methods or cocatalyst loading. Commercial strontium titanate was a UV light-active catalyst with an absorbance edge of 380 nm. Like the commercial sample, samples prepared by solid fusion and flux methods presented the primary absorbance among ultraviolet light. Compared to the absorbance band of 500–600 nm brought by the Rh^{3+} doping [30], Al^{3+} doping shows no apparent effect on creating a doping state in band positions. Furthermore, the core-shell structure of cocatalyst, $Rh@CrO_3$ on strontium titanate did not contribute to a noticeable enhancement in absorbance. The tauc plot of STSC:Al RC01 is shown in Fig. 3(b) and indicates a bandgap of 3.22 eV, which is close to 3.20 eV from commercially available strontium titanate.

Fig. 4 shows the SEM images of STSC:Al RC01. The particle size ranges from 0.5 to 1.5 μm, with only a few reaching 2–5 μm. The high

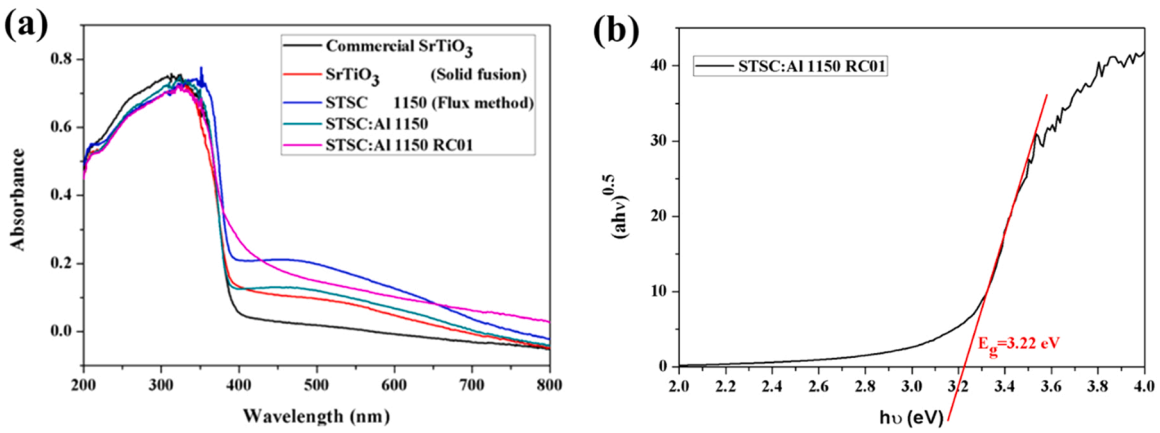

Fig. 3. (a)UV–vis spectra of commercial $SrTiO_3$, $SrTiO_3$ by solid fusion method, $SrTiO_3$ by flux method, STSC:Al by flux method, and STSC:Al RC01 with cocatalyst loading (b)Tauc plot of STSC:Al RC01.

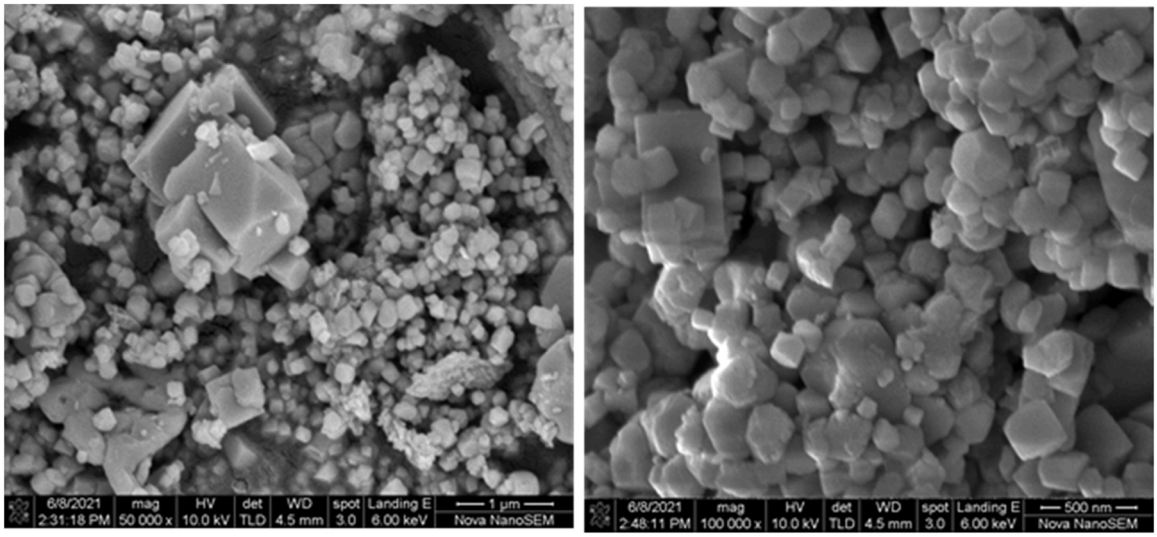

Fig. 4. FE-SEM images of STSC:Al RC01.

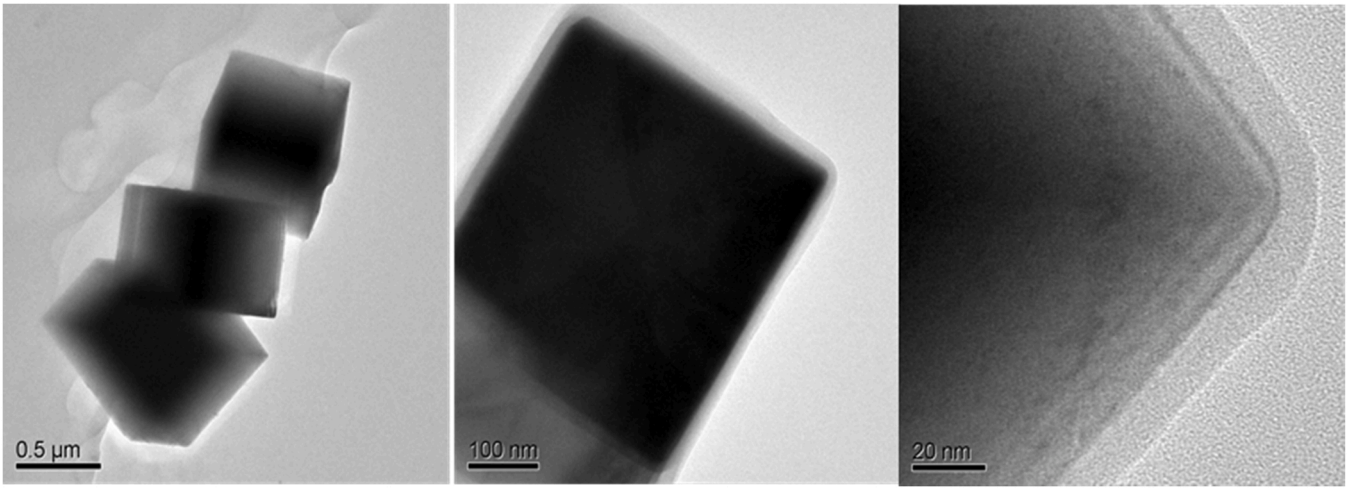

Fig. 5. HR-TEM images of STSC:Al RC01.

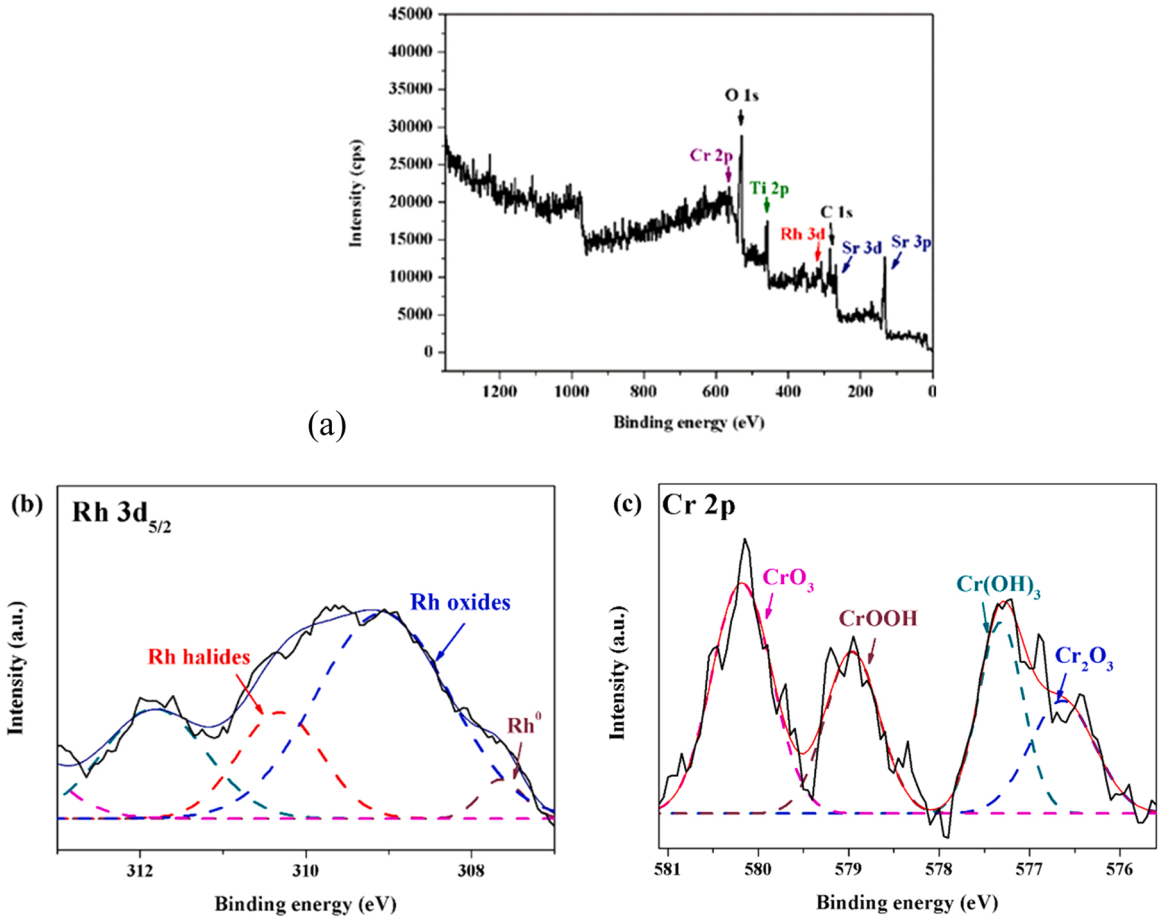

Fig. 6. XPS pattern of STSC:Al 1150 RC01, (a) survey scan, (b) Rh $3d_{5/2}$ peaks, and (c) Cr 2p peaks.

nucleation rate could explain the small particles due to increased ion diffusion in the liquid molten salt media. The truncated cubic structure was confirmed, close to previously reported literatures[26]. Since cocatalyst loading accounted for only 0.1 wt%, cocatalyst loading or surface element analysis would be further judged by HR-TEM and XPS.

TEM images of STSC:Al RC01 are displayed in Fig. 5. Since the particles were well-dispersed in strontium chloride during nucleation, no particle fusion or aggregation occurred under high heat-treatment temperature. With magnification in TEM, a clear boundary between core and shell structure on the surface of strontium titanate was observed, with a shell thickness of about 10 nm. According to reports from Yoshida et al.[18] and the usage of chromium nitrate as the precursor during impregnation, the component of the thin layer contained chromium oxide. Considering the core structure, the rhodium metal by photodeposition only accounted for 0.1 wt%, and no apparent particles could be observed in the TEM images.

To reveal the surface composition, the XPS of STSC:Al RC01 was shown in Fig. 6(a), (b), and(c). To suppress charge recombination and reverse reaction of water formation, Rh and CrO_3 were loaded step by step for the core-shell structure. Referring to Rh elemental standard

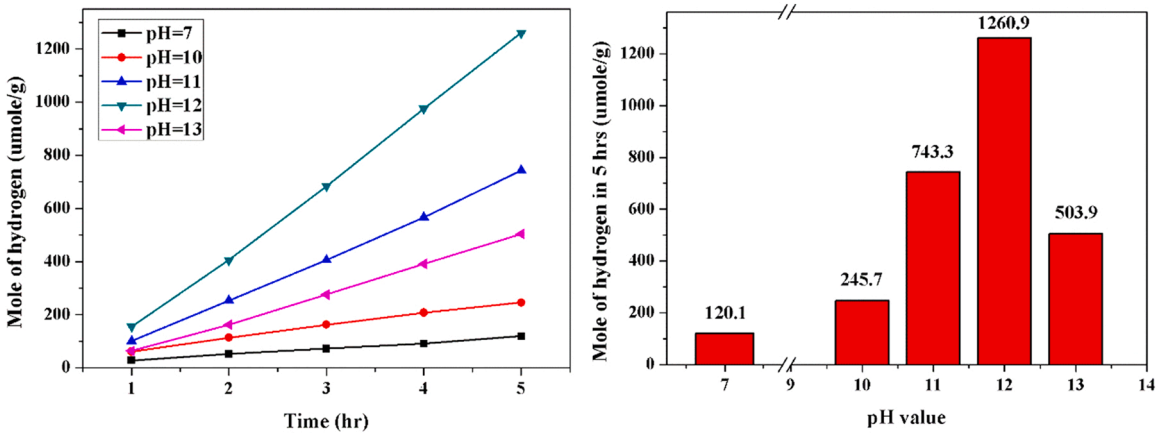

Fig. 7. (a) Time course of selective hydrogen evolution with different pH values in total five-hour irradiation (b) Comparison of total hydrogen evolution with different pH values in total five-hour irradiation (Catalyst: STSC:Al RC01; NaI concentration: 15 mM) in the single reactor.

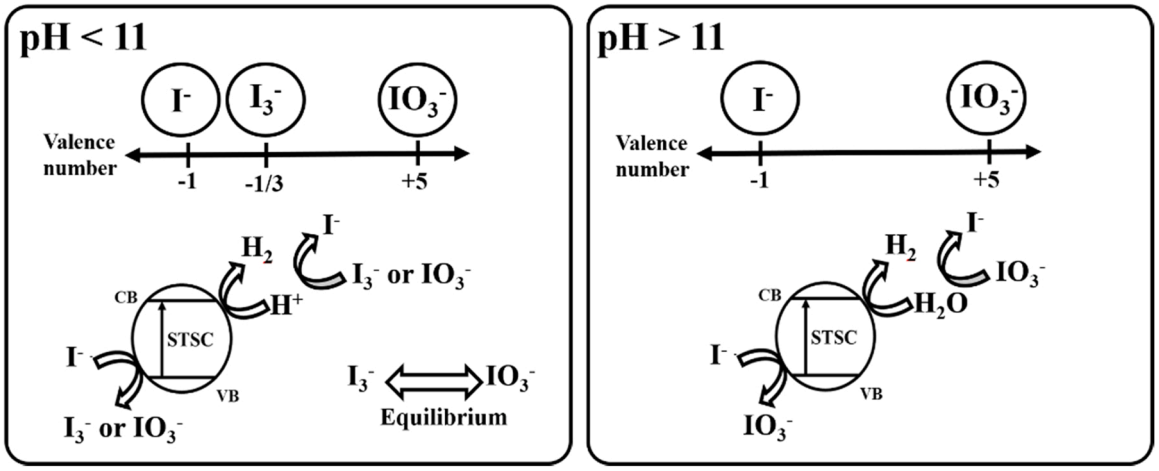

Fig. 8. Schematic illustration of possible photocatalytic reactions on the surface with pH value (a)lower than 11, (b) higher than 11.

spectrum, the binding energies of $3d_{3/2}$ and $3d_{5/2}$ orbitals fall on 312.0 eV and 307.0 eV, respectively. Fig. 6(b) shows the XPS pattern of the Rh 3d orbital. The analysis could be deconvoluted into three major peaks, 307.6 eV, 309.1 eV, and 311.8 eV. The peaks on 307.6 eV and 311.8 eV corresponds to Rh^0 metal state and composition state with halides. Since the binding energy of 309.1 eV is higher than that with Rh_2O_3. It was determined to be a mixed oxide state of Rh and Cr, which matches the previous study by Maeda et al.[27]. Fig. 6(c) shows the XPS pattern of the Cr 2p orbital. Referring to Cr elemental standard spectrum, the binding energies of $2p_{1/2}$ and $2p_{3/2}$ orbitals fall on 583.0 eV and 574.0 eV, respectively. Based on deconvolution results, the Cr elemental states on the surface show CrO_3, CrOOH, $Cr(OH)_3$, and Cr_2O_3, which fall on 580.2 eV, 579 eV, 577.3 eV, and 576.7 eV. These chemical statuses were formed by impregnation treatment during synthesis.

3.2. Half reaction of selective water splitting in a single reactor

STSC:Al RC01 was used for selective water splitting to hydrogen evolution. After the screening test, the 2 mol% Al^{3+} doped catalyst gave the highest activity of pure water splitting, as shown in Fig.S5, so only this catalyst was further studied. The iodide ion (I^-) was used as a sacrificial agent in the system. The reactions involved are shown in Eqs. (1)–(3) or Eqs. (4)–(6), depending on the pH value. Upon photocatalyst absorbing light irradiation, photoinduced electron-hole pairs can be generated and perform a photocatalytic reaction after migrating to the surface. Eqs. (1)–(3) shows the mechanism in the neutral condition. Protons can be reduced by electrons into hydrogen molecules, while iodide molecules consume surplus holes and are oxidized into iodate molecules to prevent charge recombination. Eqs. (4)–(6) present the mechanism in basic conditions. Water molecules can be reduced by electrons into hydrogen molecules and hydroxyl ions, while iodide molecules still behave as reducing agents to remove photoinduced holes.

$$SrTiO_3 + h\nu \rightarrow e^- + h^+ \quad (1)$$

$$6\,H^+ + 6e^- \rightarrow 3\,H_2 \quad (2)$$

$$I^- + 6\,h^+ + 3\,H_2O \rightarrow 6\,H^+ + IO_3^- \quad (3)$$

$$SrTiO_3 + h\nu \rightarrow e^- + h^+ \quad (4)$$

$$6\,H_2O + 6e^- \rightarrow 3\,H_2 + 6OH^- \quad (5)$$

$$I^- + 6OH^- + 6\,h^+ \rightarrow IO_3^- + 3\,H_2O \quad (6)$$

Fig. 7 shows the effect of pH value on hydrogen evolution per gram catalyst in five-hour irradiation with iodide ion as the sacrificial agent. Among all the cases, pH 12 led to the highest evolution with 1260 μmole hydrogen per gram catalyst with no oxygen being evolved and detected. Compared to whole water splitting shown in Fig.S6, the introduction of iodide ion boosted a 9.1% increase in hydrogen production. It served to prove successful selective water splitting. Interestingly, under neutral condition, hydrogen evolution from selective water splitting showed nearly ten times lower than that in whole water splitting, even with I^- as the sacrificial agent. Abe et al.[31] reported the pH value effect on I^-/IO_3^- system during the photocatalytic reaction, presented in Fig. 8. When the pH value is lower than 11, the reactions are shown in Eqs. (7)-(10). In addition to the oxidation into iodate ions by photoinduced holes, iodide ions stand a chance to be oxidized into I_2 and combined with I^- to form I_3^-. Since the valence number of I_3^- shows − 1/3, it stands a chance to consume the photoinduced electrons. Thus the competition reactions between I_3^- and protons towards electrons could be unpreventable, resulting in low water splitting efficiency. In contrast, when the pH value is higher than 11, the oxidation of iodide ions into triiodide ions will be suppressed and resume the high photocatalytic performance. As for the decrease of hydrogen evolution in pH values higher than 12, Fig. 9 shows the H_2 yields of whole water splitting before and after testing under selective water splitting. Although the decrease in activity is confirmed, the hydrogen evolution still increases stably with time. Part of chromium oxide might be dissolved in solution during the strong basic condition due to chromium being an amphoteric element.

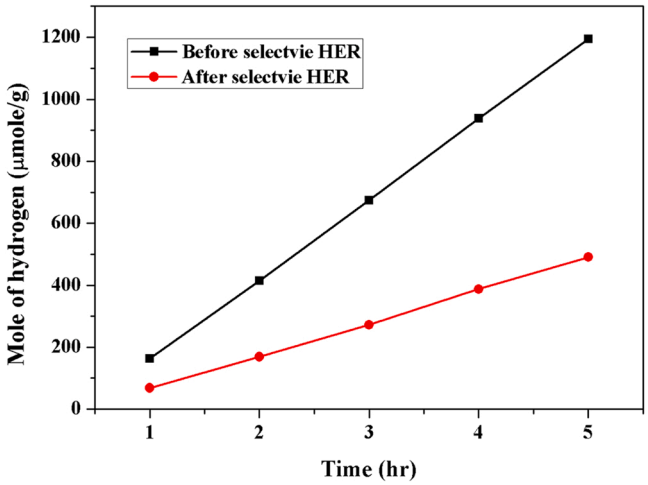

Fig. 9. Comparison of hydrogen evolution with whole water splitting before and after selective water splitting under pH= 13 (Catalyst: STSC:Al RC01).

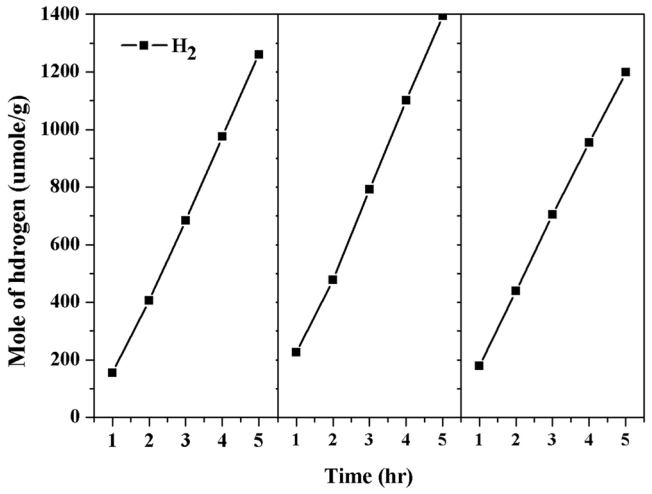

Fig. 10. Stability test with STSC:Al RC01 under selective water splitting. (pH value:12; NaI concentration: 15 mM).

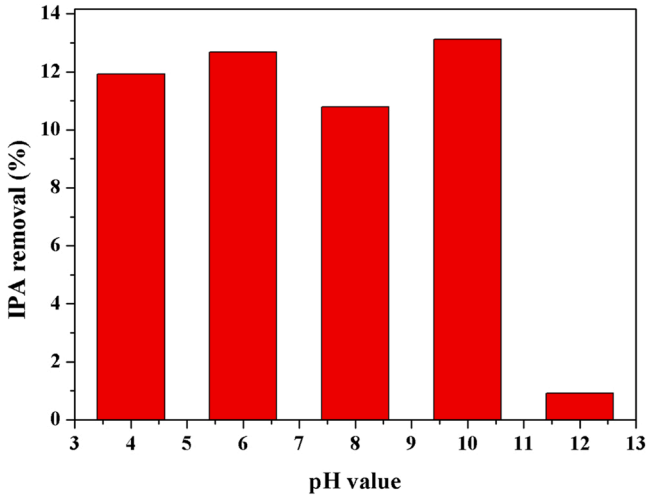

Fig. 11. Comparison of total isopropanol degradation in selective IPA degradation with different pH value in total five-hour irradiation (Catalyst:Pt/WO_3; $NaIO_3$ concentration: 15 mM).

$$I^- + 6\,h^+ + 3\,H_2O \rightarrow 6\,H^+ + IO_3^- \quad (7)$$

$$2I^- + 2\,h^+ \rightarrow I_2\ (\text{or } I_3^-) \quad (8)$$

$$2\,H^+ + 2e^- \rightarrow H_2 \quad (9)$$

$$I_2\ (\text{or } I_3^-) + 2e^- \rightarrow 2\,I^- \quad (10)$$

To evaluate stability, the catalyst is recycled from the reaction in pH= 12, washed with DI water, and dried in the oven under 60 ℃ overnight. Afterward, the stability test was conducted for three cycles, as shown in Fig. 10. After three cycles, STSC:Al RC01 maintained excellent activity for water splitting without evident decline. Furthermore, the average hydrogen evolution in selective water splitting increased by 9.1% compared to that in whole water splitting, showing the increment brought by adding iodide ions. Based on the optimization, the best parameter in the half-reaction of water splitting was pH= 12.

3.3. Half reaction of isopropanol degradation in a single reactor

For selective isopropanol degradation, Pt/WO_3 was used. The initial isopropanol concentration was set to 100 ppm. In order to perform the

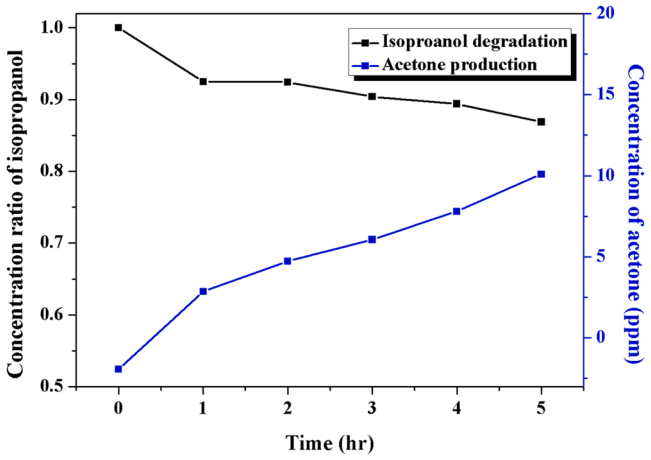

Fig. 12. Isopropanol concentration ratio and acetone production in total 5-hour irradiation with the original IPA concentration of 100 ppm (Catalyst: Pt/WO_3; pH value: 10; $NaIO_3$ concentration: 15 mM).

Z-scheme system in the twin reactor, the usage of IO_3^- on the isopropanol degradation side was coupled with I^- on the hydrogen evolution side. The reactions involved are shown in Eqs. (11)-(14). Upon photocatalyst absorbing light irradiation, photoinduced electron-hole pairs can be produced. Holes can oxidize hydroxyl ions into hydroxyl radicals, which is highly oxidative. Then hydroxyl radicals can oxidize isopropanol molecules into mainly acetone molecules. At the same time, iodate molecules consume surplus electrons and are reduced into iodide molecules to prevent charge recombination. Fig. 11 displays the effect of pH value on photocatalytic isopropanol degradation. Among all the selected conditions, the highest 13.1% removal ratio was at pH= 10. The concentration of hydroxyl ion was enhanced with the increase in pH value, which facilitates the possibility of hydroxyl ion formation by photoinduced holes. That is, the oxidation was enhanced with pH value in the case. Conversely, tungsten oxide was dissolved in strong basic condition, which could be proven by the dramatic decrease in the IPA removal ratio under pH at 12. Based on the optimization, the best parameter in half-reaction of IPA degradation fell on pH= 10.

$$Pt/WO_3 + h\nu \rightarrow e^- + h^+ \quad (11)$$

$$OH^- + h^+ \rightarrow OH\bullet \quad (12)$$

$$2\,OH\bullet + C_3H_8O \rightarrow C_3H_6O + 2\,H_2O \quad (13)$$

$$IO_3^- + 3\,H_2O + 6e^- \rightarrow I^- + 6OH^- \quad (14)$$

$$Isopropanol \xrightarrow{OH\bullet} Acetone \xrightarrow{OH\bullet} Intermediates \xrightarrow{OH\bullet} CO_2 \quad (15)$$

Fig. 12 shows the time course of isopropanol degradation and

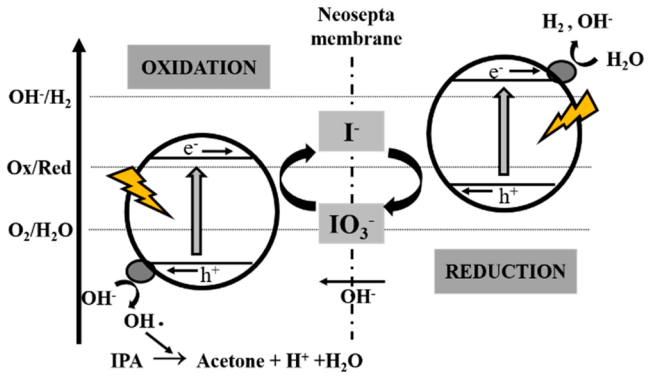

Fig. 13. H_2 evolution and IPA degradation using 15 mM I^-/IO_3^- in twin reactors.

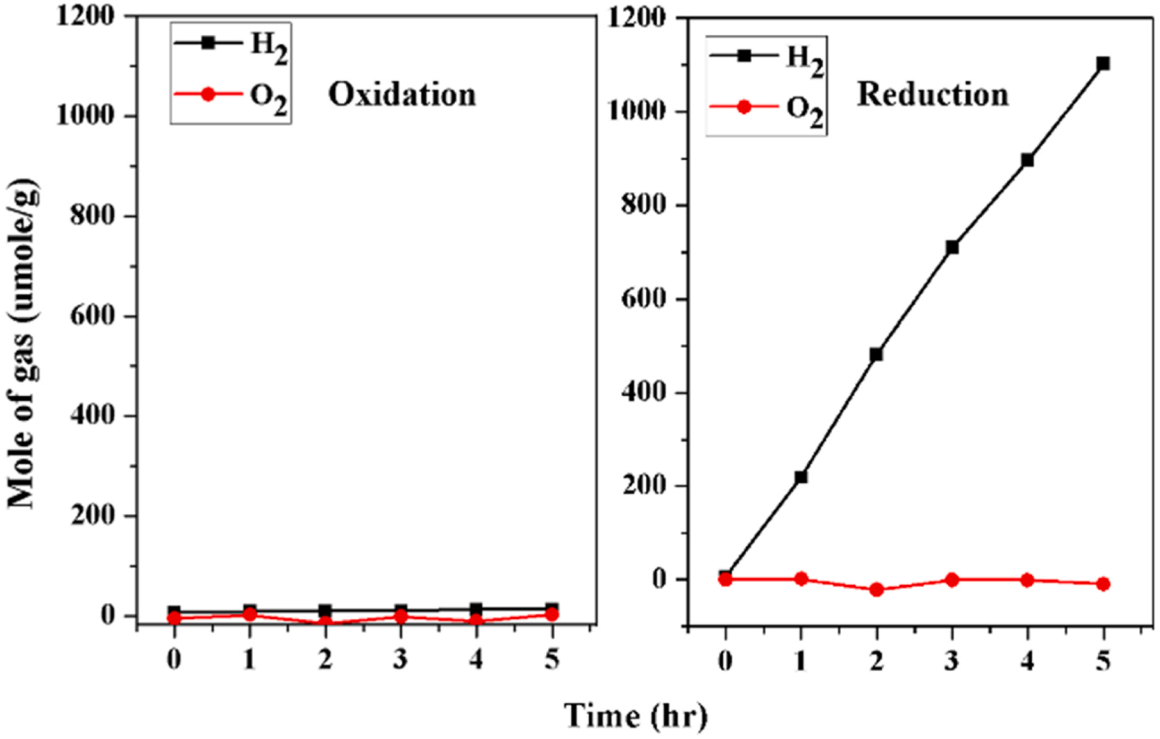

Fig. 14. Gas evolution on both sides in twin reactors using 15 mM I^-/IO_3^-.

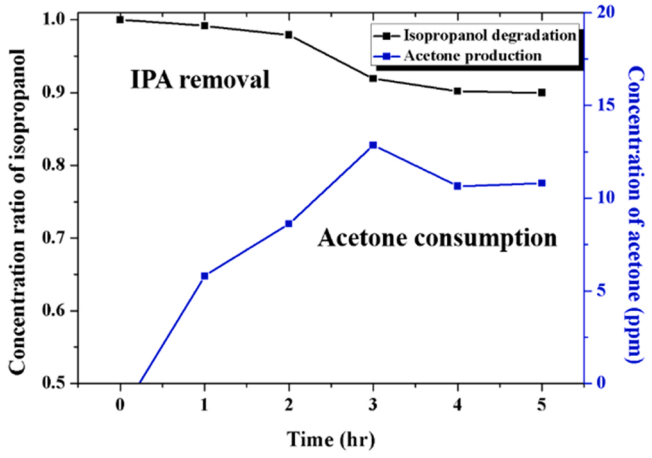

Fig. 15. IPA degradation and Acetone evolution on oxidation side using 15 mM I^-/IO_3^- (pH value for oxidation side: 10).

acetone conversion under pH= 10. A 13.1% IPA removal and 10 ppm of acetone were reached under pH= 10 in five-hour irradiation. The intermediate product of isopropanol degradation was acetone, with a few of them being further oxidized into acetic acid or carbon dioxide [32]. Eq. (15) indicates that the degradation of isopropanol into minor organic compounds are series reaction. The converted acetone can compete with isopropanol for photoinduced holes, so the IPA degradation rate slows down as time passes.

3.4. Twin photoreactions in the twin reactor

The design of twin reactors is inspired by the Z-scheme system in the chloroplast, where oxygen or glucose is separately oxidized from water or reduced from carbon dioxide. In this study, the schematic illustration of the twin reactor is shown in Fig. 1(b). Two chambers are separated by the Neosepta anion-exchanged membrane. With STSC:Al RC01 and Pt/WO_3 being placed on either side in the twin reactor, photocatalytic water splitting into hydrogen and isopropanol degradation are expected to co-occur. On the hydrogen evolution side, 0.1 g of STSC:Al RC01, 15 mM NaI, and 200 mL water solution was prepared, and the pH value was adjusted to 12. On the IPA degradation side, 0.1 g of Pt/WO_3, 15 mM $NaIO_3$, 100 ppm, and 200 mL water solution was prepared, and the pH value was adjusted to 10.

Fig. 13 demonstrates the mechanism of how the twin reactor works. Upon absorbing light irradiation, photocatalysts on both sides were activated for photoreactions. On the hydrogen evolution side, hydrogen is produced with I^- to be converted into IO_3^-. While on the IPA degradation side, isopropanol is degraded by hydroxyl radical originating from photocatalytic reaction with holes. Iodate ions (IO_3^-) behave as reducing agents to facilitate charge separation. During photocatalysis, the concentration gradients of produced I^- or IO_3^- between two chambers will counter-diffuse through the anion exchange membrane to meet the charge balance and mass balance. Fig. 14 and Fig. 15 show the gas-phase products and liquid-phase composition on two sides of the twin reactor, respectively. In five-hour irradiation, a hydrogen evolution rate of about 220 μmole H_2/gram catalyst/hr was achieved on the hydrogen evolution side, while no hydrogen was evolved on the IPA degradation side, as shown in Fig. 14. The result proved the successful separation of produced hydrogen in the twin reactor. As for liquid-phase composition, around 10.1% of isopropanol removal and 10.8 ppm of acetone conversion are recognized, as shown in Fig. 15. Concerning the time course of acetone concentration, the acetone concentration peaked at the third hour and kept stable in the following hours. It proved the competitive mechanism between isopropanol, acetone, and minor organic compounds toward photoinduced hydroxyl radicals.

(pH value for reduction side: 12; pH value for oxidation side: 10).

3.5. Kinetics investigation in the twin reactor

Hydrogen was generated and separated in the twin photoreactor. However, hydrogen evolution and IPA degradation were decreased by

Table 2
Comparison of reaction rate in twin concerning I^-/IO_3^- consumption.

	Twin reactor with H_2 evolution and IPA degradation
Hydrogen evolution rate (μmole of I^-/hr)	7.35
Diffusion rate (μmole of IO_3^-/hr)	176
IPA degradation rate (μmole of IO_3^-/hr)	9.09

12.6% and 3.1%, respectively, compared with the results in the half-reaction in the single reactor. To determine the rate-determining step in the system, kinetics should be considered. Based on the charge balance on the catalyst, the photocatalytic reaction is presented by the consumption rate of electron mediators, I^- or IO_3^- on two sides in the twin reactor. The anion diffusion rate on the anion exchange membrane was measured and its diffusivity was calculated by Fick's law, as shown in Eqs. 16–19 (see Supplementary Information). Reaction rates in each compartment of the twin reactor are summarized in Table2. Hydrogen evolution rate and IPA degradation rate are calculated to be 7.35 μmole I^-/hr and 9.09 μmole IO_3^-/hr, which are much less than that of the anion diffusion rate through the anion membrane. Thus, the twin reactor is kinetically controlled.

$$Iodide\quad comsuption\quad rate\left(\frac{\mu mole}{hr}\right)=\frac{1}{3}X(Hydrogen\quad evolution\quad rate)\left(\frac{\mu mole}{g\bullet hr}\right)X\quad gram\quad of\quad catalyst(g) \tag{16}$$

$$Iodate\quad comsuption\quad rate\left(\frac{\mu mole}{hr}\right)=\frac{2}{3}X(Oxygen\quad evolution\quad rate)\left(\frac{\mu mole}{g\bullet hr}\right)X\quad gram\quad of\quad catalyst(g) \tag{17}$$

$$Iodate\quad comsuption\quad rate\left(\frac{\mu mole}{hr}\right)=\frac{1}{3}X(IPA\quad degradation\quad rate)\left(\frac{\mu mole}{g\bullet hr}\right)X\quad gram\quad of\quad catalyst(g) \tag{18}$$

$$Iodate\quad diffusion\quad rate\left(\frac{\mu mole}{hr}\right)=Diffusivity\quad X\quad Area\quad of\quad membran\left(cm^2\right)\quad X\quad concentration\quad gradient\left(\frac{M}{cm}\right) \tag{19}$$

4. Conclusions

Photocatalytic water splitting was performed by core-shell structural Rh-CrO_x loaded, Al^{3+} doped strontium titanate with iodide ion as the sacrificial agent. To prevent the side reactions brought by I_3^-, the basic condition of pH= 12 should be conducted. Hydrogen yield of 252 μmole/gram catalyst/hr and quantum efficiency of 0.117% were obtained in half-reaction of selective water splitting. Secondly, a specially designed twin reactor was used for simultaneous hydrogen evolution and IPA degradation with the usage of electron mediators, I^-/IO_3^-. In five-hour irradiation, the quantum efficiency of 0.102% and 0.123% were reached on the hydrogen evolution side and IPA degradation side. With the help of I^-/IO_3^-, reduction and oxidation were performed on the individual side in twin reactors, leading to the separation of produced hydrogen and saving on hydrogen purification costs. With the kinetic analysis, the system showed kinetically controlled, as photocatalytic reactions behaved as the rate-determining steps. Our study demonstrated that the twin photoreactor can generate pure hydrogen and degrade wastewater simultaneously, thus having a high potential for hydrogen production from water splitting by sunlight harvesting.

CRediT authorship contribution statement

Yu-Yang Tai: Investigation, Data curation and Writing – original draft, **Jeffrey C. S. Wu:** Conceptualization, Supervision, Methodology, Writing – review & editing, **Wen-Yueh Yu:** Resources and Validation, **Marjeta Maček Kržmanc:** Investigation, Data curation, Validation, **Eugene Kotomin:** Resources and Validation.

Declaration of Competing Interest

The authors declare that they have no known competing financial interests or personal relationships that could have appeared to influence the work reported in this paper.

Data Availability

Data will be made available on request.

Acknowledgment

The authors gratefully acknowledge the Ministry of Science and Technology (MOST), Taiwan, for the financial support under grant

number MOST 108-2923-E-002-006-MY3. M.M.K. acknowledges the Ministry for Education, Science, and Sport from Slovenia to provide support for M-era.Net project (SunToChem), under contract no. C3330-19-252011). The EK study was performed with partial financial support from the FLAG ERA JTC project To2DOx.The Institute of Solid State Physics, University of Latvia (Latvia), as the Centre of Excellence, has received funding from the European Union's Horizon 2020 Frame-work Programme H2020-WIDESPREAD-01-2016-2017-Teaming Phase2 under grant agreement No. 739508, project CAMART2. The authors thank L. Rusevich and G. Zvejnieks of the University of Latvia for stimulating discussions. Dr. Nina Daneu of the Jožef Stefan Institute is highly appreciated for the STEM of STSC:Al catalyst.

Appendix A. Supporting information

Supplementary data associated with this article can be found in the online version at doi:10.1016/j.apcatb.2022.122183.

References

[1] T. Su, Q. Shao, Z. Qin, Z. Guo, Z. Wu, Role of interfaces in two-dimensional photocatalyst for water splitting, ACS Catal. 8 (2018) 2253–2276.
[2] A. Kudo, Y. Miseki, Heterogeneous photocatalyst materials for water splitting, Chem. Soc. Rev. 38 (2009) 253–278.
[3] S. Escobedo Salas, Photocatalytic Water Splitting using a Modified Pt-TiO2. Kinetic Modeling and Hydrogen Production Efficiency, Elect. Thesis Diss. Repos. 1475. (2013). https://ir.lib.uwo.ca/etd/1475.
[4] B. Weng, J. Wu, N. Zhang, Y.-J. Xu, Observing the role of graphene in boosting the two-electron reduction of oxygen in graphene–WO3 nanorod photocatalysts, Langmuir 30 (2014) 5574–5584.
[5] L. Zheng, H. Su, J. Zhang, L.S. Walekar, H.V. Molamahmood, B. Zhou, M. Long, Y. H. Hu, Highly selective photocatalytic production of H2O2 on sulfur and nitrogen co-doped graphene quantum dots tuned TiO2, Appl. Catal. B Environ. 239 (2018) 475–484.
[6] N. Ambrožová, M. Reli, M. Šihor, P. Kuśtrowski, J.C. Wu, K. Kočí, Copper and platinum doped titania for photocatalytic reduction of carbon dioxide, Appl. Surf. Sci. 430 (2018) 475–487.
[7] A. Ajmal, I. Majeed, R.N. Malik, H. Idriss, M.A. Nadeem, Principles and mechanisms of photocatalytic dye degradation on TiO 2 based photocatalysts: a comparative overview, RSC Adv. 4 (2014) 37003–37026.
[8] U. Aftab, A. Tahira, A. Gradone, V. Morandi, M.I. Abro, M.M. Baloch, A.L. Bhatti, A. Nafady, A. Vomiero, Z.H. Ibupoto, Two step synthesis of TiO2–Co3O4 composite for efficient oxygen evolution reaction, Int. J. Hydrog. Energy 46 (2021) 9110–9122.
[9] J. Liu, Y. Zou, B. Jin, K. Zhang, J.H. Park, Hydrogen peroxide production from solar water oxidation, ACS Energy Lett. 4 (2019) 3018–3027.
[10] R. Konta, T. Ishii, H. Kato, A. Kudo, Photocatalytic activities of noble metal ion doped SrTiO3 under visible light irradiation, J. Phys. Chem. B 108 (2004) 8992–8995.
[11] C. Wang, H. Qiu, T. Inoue, Q. Yao, Band gap engineering of SrTiO3 for water splitting under visible light irradiation, Int. J. Hydrog. Energy 39 (2014) 12507–12514.
[12] T. Takata, K. Domen, Defect engineering of photocatalysts by doping of aliovalent metal cations for efficient water splitting, J. Phys. Chem. C. 113 (2009) 19386–19388.
[13] J. Meng, Q. Lin, T. Chen, X. Wei, J. Li, Z. Zhang, Oxygen vacancy regulation on tungsten oxides with specific exposed facets for enhanced visible-light-driven photocatalytic oxidation, Nanoscale 10 (2018) 2908–2915.
[14] A. Iwase, H. Kato, A. Kudo, Nanosized Au particles as an efficient cocatalyst for photocatalytic overall water splitting, Catal. Lett. 108 (2006) 7–10.
[15] Y. Inoue, Photocatalytic water splitting by RuO 2-loaded metal oxides and nitrides with d 0-and d 10-related electronic configurations, Energy Environ. Sci. 2 (2009) 364–386.
[16] R. Li, F. Zhang, D. Wang, J. Yang, M. Li, J. Zhu, X. Zhou, H. Han, C. Li, Spatial separation of photogenerated electrons and holes among {010} and {110} crystal facets of BiVO 4, Nat. Commun. 4 (2013) 1–7.
[17] J. Liu, Q. Jia, J. Long, X. Wang, Z. Gao, Q. Gu, Amorphous NiO as co-catalyst for enhanced visible-light-driven hydrogen generation over g-C3N4 photocatalyst, Appl. Catal. B Environ. 222 (2018) 35–43.
[18] M. Yoshida, K. Takanabe, K. Maeda, A. Ishikawa, J. Kubota, Y. Sakata, Y. Ikezawa, K. Domen, Role and function of noble-metal/Cr-layer core/shell structure cocatalysts for photocatalytic overall water splitting studied by model electrodes, J. Phys. Chem. C 113 (2009) 10151–10157.
[19] J. Boltersdorf, N. King, P.A. Maggard, Flux-mediated crystal growth of metal oxides: synthetic tunability of particle morphologies, sizes, and surface features for photocatalysis research, CrystEngComm 17 (2015) 2225–2241.
[20] H. Kato, M. Kobayashi, M. Hara, M. Kakihana, Fabrication of SrTiO 3 exposing characteristic facets using molten salt flux and improvement of photocatalytic activity for water splitting, Catal. Sci. Technol. 3 (2013) 1733–1738.
[21] M. Shaban, A.M. Ashraf, M.R. Abukhadra, TiO 2 nanoribbons/carbon nanotubes composite with enhanced photocatalytic activity; fabrication, characterization, and application, Sci. Rep. 8 (2018) 1–17.
[22] Q. Su, Y. Li, R. Hu, F. Song, S. Liu, C. Guo, S. Zhu, W. Liu, J. Pan, Heterojunction photocatalysts based on 2D materials: the role of configuration, Adv. Sustain. Syst. 4 (2020), 2000130.
[23] M. Maček Kržmanc, N. Daneu, A. Čontala, S. Santra, K.M. Kamal, B. Likozar, M. Spreitzer, SrTiO3/Bi4Ti3O12 nanoheterostructural platelets synthesized by topotactic epitaxy as effective noble-metal-free photocatalysts for ph-neutral hydrogen evolution, ACS Appl. Mater. Interfaces 13 (2021) 370–381.
[24] S. Berardi, S. Drouet, L. Francàs, C. Gimbert-Suriñach, M. Guttentag, C. Richmond, T. Stoll, A. Llobet, Molecular artificial photosynthesis, Chem. Soc. Rev. 43 (2014) 7501–7519.
[25] S.-C. Yu, C.-W. Huang, C.-H. Liao, J.C. Wu, S.-T. Chang, K.-H. Chen, A novel membrane reactor for separating hydrogen and oxygen in photocatalytic water splitting, J. Membr. Sci. 382 (2011) 291–299.
[26] Y. Ham, T. Hisatomi, Y. Goto, Y. Moriya, Y. Sakata, A. Yamakata, J. Kubota, K. Domen, Flux-mediated doping of SrTiO 3 photocatalysts for efficient overall water splitting, J. Mater. Chem. A 4 (2016) 3027–3033.
[27] K. Maeda, D. Lu, K. Teramura, K. Domen, Direct deposition of nanoparticulate rhodium–chromium mixed-oxides on a semiconductor powder by band-gap irradiation, J. Mater. Chem. 18 (2008) 3539–3542.
[28] U.A. Joshi, J.R. Darwent, H.H. Yiu, M.J. Rosseinsky, The effect of platinum on the performance of WO3 nanocrystal photocatalysts for the oxidation of Methyl Orange and iso-propanol, J. Chem. Technol. Biotechnol. 86 (2011) 1018–1023.
[29] T. Alammar, V. Smetana, H. Pei, I. Hamm, M. Wark, A.V. Mudring, The power of ionic liquids: crystal facet engineering of SrTiO3 nanoparticles for tailored photocatalytic applications, Adv. Sustain. Syst. 5 (2021), 2000180.
[30] Y.-T. Lin, Y.-H. Wang, J.C. Wu, X. Wang, Photo-Fenton enhanced twin-reactor for simultaneously hydrogen separation and organic wastewater degradation, Appl. Catal. B Environ. 281 (2021), 119517.
[31] R. Abe, K. Sayama, K. Domen, H. Arakawa, A new type of water splitting system composed of two different TiO2 photocatalysts (anatase, rutile) and a IO3−/I− shuttle redox mediator, Chem. Phys. Lett. 344 (2001) 339–344.
[32] J.M. Coronado, S. Kataoka, I. Tejedor-Tejedor, M.A. Anderson, Dynamic phenomena during the photocatalytic oxidation of ethanol and acetone over nanocrystalline TiO2: simultaneous FTIR analysis of gas and surface species, J. Catal. 219 (2003) 219–230.